Supplementary report for "Human multi-robot safe interaction: a trajectory scaling approach based on safety assessment"

Analysis of different human safety assessment formulations in the trajectory scaling approach

by Martina Lippi, Alessandro Marino

In this document, alternative formulations for the cumulative safety index are analyzed and are shown to be inappropriate for performing trajectory scaling. In particular, the following cases are considered:

1. trajectory scaling considering only the safety index relative to the closest robot;
2. trajectory scaling considering only the minimum safety field robot.

The two solutions are discussed in the following and illustrative simulations are provided. The same set of parameters used in the simulation case study of the paper is assumed, unless otherwise specified.

Closest robot approach

In this scenario, we consider the robot i_c with minimum distance with respect to the human operator

$$i_c = \min_{i \in \{1,\dots,N\}} d^* \qquad \text{with} \qquad d^* = \min_{\forall i,l,s,j} \|\boldsymbol{p}^s_{i,l} - \boldsymbol{p}_{o,j}\| \quad \text{as in } (12)_{\text{r}} \tag{E1}$$

and we assume that the safety field and coefficients μ_1 and μ_2 associated to the system are those relative to the closest robot, that is:

$$\bar{F} = \bar{F}_{i_c}, \quad \mu_1 = \mu_{1,i_c}, \quad \mu_2 = \mu_{2,i_c} \tag{E2}$$

which are, thus, used to perform the trajectory scaling approach described in Section IV-B and in lieu of the sum of the safety indices relative to all robots as in the proposed approach.
To prove that the above formulation is not suitable for a multi-robot collaborative scenario, we provide a simulation case study where the safety index in (E2) is shown to jump in a discontinuous manner from a value to a lower one, thus preventing the safety condition from being guaranteed.

More specifically, let us consider the setup depicted in Figure 1 involving two robots ($N = 2$) and let us assume the human operator stands in the work-cell without moving, while robot 2 moves towards robot 1, which is still. The nominal trajectory is reported in Figure 2 and, with no loss of generality, a single representative point is considered for the human with position $\boldsymbol{p}_o(t) = \begin{bmatrix} 2.0 & -1.2 & 1.2 \end{bmatrix}^T$, $\forall t$.

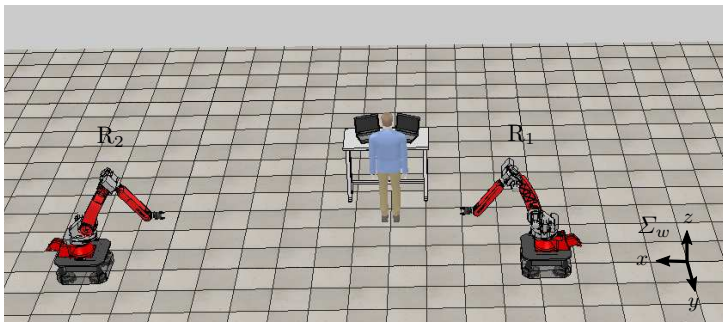

Figure 1: Closest robot approach. Simulation setup composed of 2 robots (R_i, $i = 1, 2$) and a human operator; the world reference frame Σ_w is shown.

Snapshots of the system behavior are shown in Figure 3, while results are reported in Figures 4-5. The index i_c of the closest robot at each time is shown in Figure 4 and, as robot 2 approaches the human operator, the index i_c is shown to switch from 1 to 2 at time $t = 5.8$ s. The individual safety functions $\bar{F}_i$, $i = 1, 2$ (dotted lines) as well as the overall safety function $\bar{F}$ in (E2) (solid line) are reported in Figure 5. In particular, the latter makes evident that, as soon as i_c switches, the overall safety $\bar{F}$ switches as well

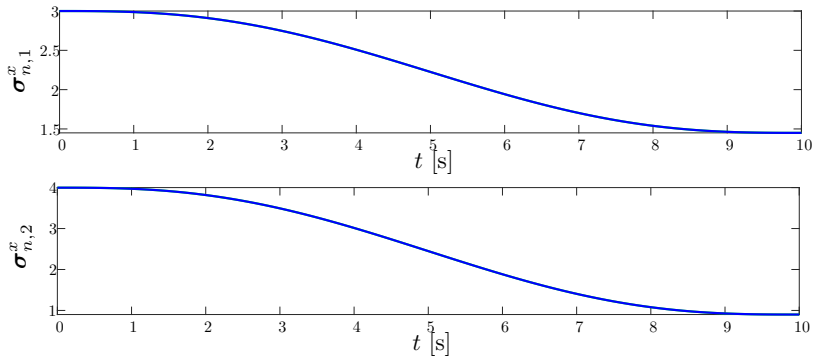

Figure 2: Closest robot approach. Evolution of the nominal trajectory; in detail, the positional components along x of the team centroid $\boldsymbol{\sigma}_1$ and formation $\boldsymbol{\sigma}_2$ are shown (namely, $\boldsymbol{\sigma}^x_{n,1}$, $\boldsymbol{\sigma}^x_{n,2}$). The remaining components are kept constant.

from $\bar{F}_1 = 14.9$ to $\bar{F}_2 = 12.2$. This implies that it is not possible to guarantee a minimum safety $\bar{F}_{min}$ in the range $(14.9, 12.2)$ as the safety function discontinuously jump to a value $\bar{F} < \bar{F}_{min}$, thus violating the safety condition. Note that, in Figure 5, although both human and robot 1 do not move, $\bar{F}_1$ increases thanks to the null space action as described in Section V.

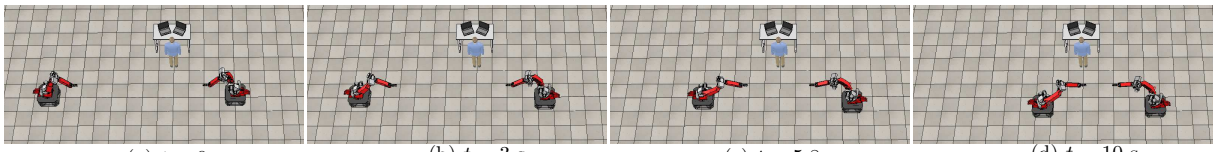

(a) $t = 0$ s (b) $t = 3$ s (c) $t = 5.8$ s (d) $t = 10$ s

Figure 3: Closest robot approach. Snapshots of the key phases of the simulation: the initial configuration of the work-cell is in Figure (a); robot 2 moves towards robot 1 while robot 1 moves in the null space in Figure (b); robot 2 becomes the closest robot in Figure (c), final configuration in Figure (d).

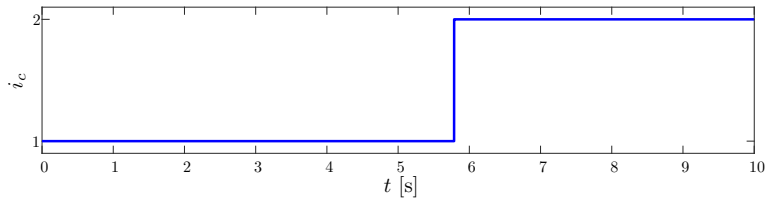

Figure 4: Closest robot approach. Index of the closest robot i_c.

On the contrary, by considering the cumulative safety index presented in the paper, i.e. $\bar{F} = \sum_{i=1}^{N} \bar{F}_i$, the aforementioned problem does not arise by construction and the task can be successfully accomplished by meeting constraints on the minimum safety field.
In order to show this, the case of $\bar{F}_{min} = 27.1$, corresponding to sum of the safety fields at the aforementioned switching time $t = 5.8$ s, has been considered in the case of our approach, and the resulting safety index is shown in Figure 6. In particular, in the time interval [5.8, 17.7] s, the safety index is saturated at the minimum value and the trajectory is decelerated. Then, once the safety condition is fulfilled again, the task is recovered. The scaling parameters c (in blue) and derivatives are reported in Figure 7 compared to their nominal values (in green) to show how the trajectory is modulated, while the resulting reference trajectory (in blue with respect to the nominal one in green) is reported in Figure 8.

Finally, it is worth noticing that the adoption of the formulation in (E2) would also not be appropriate for a distributed framework as it would require the dynamic tracking of a minimum value of the network, that is still an open question in current distributed control community.

Minimum safety robot approach

In this approach the overall safety field of the multi-robot system is equal to minimum robot field. In detail, let us consider the robot i_f with minimum safety index and define the overall safety index

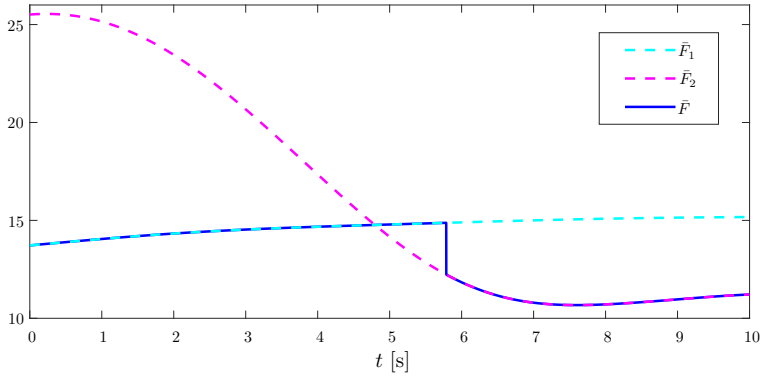

Figure 5: Closest robot approach. Evolution of the overall safety function $\bar{F}$ (solid line in blue) and of the local safety functions $\bar{F}_1$ and $\bar{F}_2$ (dotted cyan and magenta lines respectively).

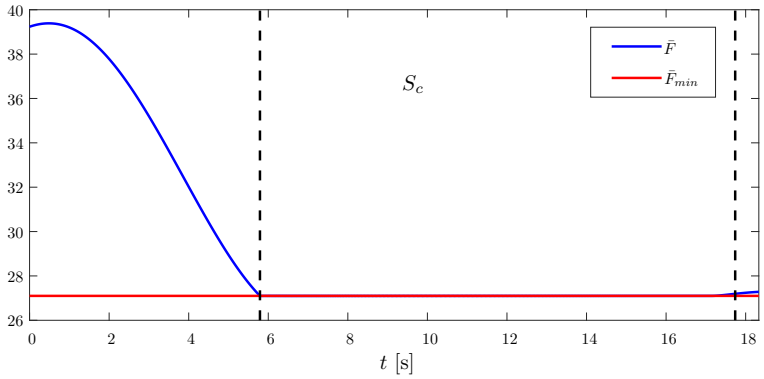

Figure 6: Our method in the setting of the closest robot approach. Evolution of the overall safety function $\bar{F}$ (in blue) with respect to the minimum value $\bar{F}_{min}$ (in red). The scaling phase is highlighted with notation S_c.

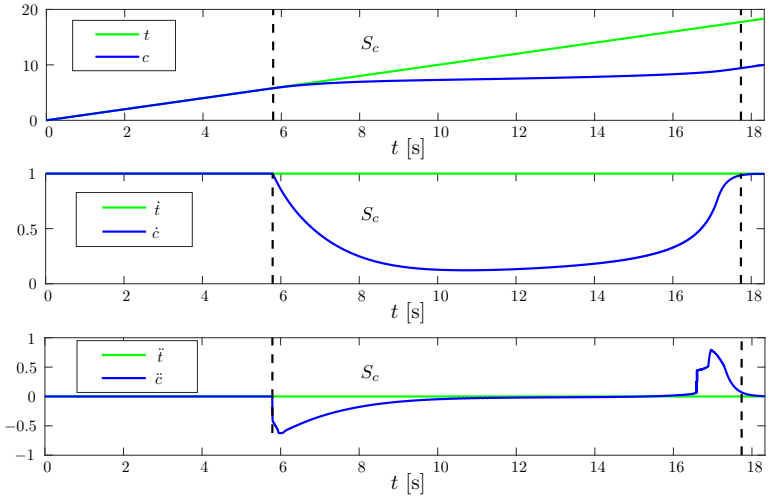

Figure 7: Our method in the setting of the closest robot approach. Evolution of the scaling parameters $c(t)$, $\dot{c}(t)$, $\ddot{c}(t)$ (in blue) compared with their nominal values (in green); scaling phase is highlighted with S_c.

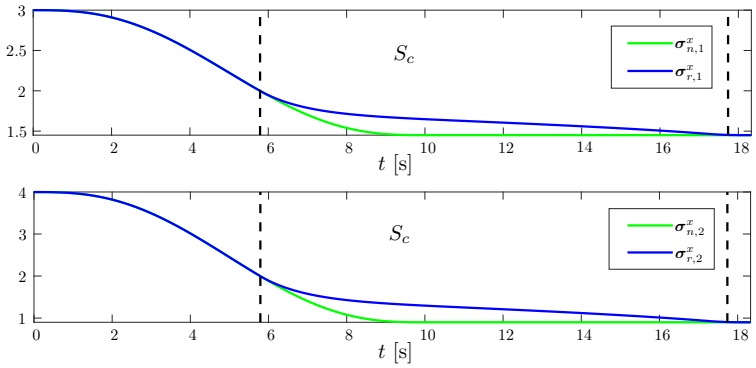

Figure 8: Our method in the setting of the closest robot approach. Evolution of the nominal (n, in green) and reference (r, in blue) trajectories; in detail, the positional components along x of the team centroid $\boldsymbol{\sigma}_1$ and formation $\boldsymbol{\sigma}_2$ are shown (namely, $\boldsymbol{\sigma}^x_{k,1}$, $\boldsymbol{\sigma}^x_{k,2}$ with $k = n, r$). The remaining components are kept constant while scaling phase is marked with S_c.

accordingly, i.e.

$$\bar{F} = \bar{F}_{i_f} \qquad \text{with} \qquad i_f = \min_{i \in \{1,\dots,N\}} \bar{F}_i \tag{E3}$$

The trajectory scaling method presented in Section IV-B is applied using coefficients $\mu_1 = \mu_{1,i_f}$ and $\mu_2 = \mu_{2,i_f}$.

As shown in the following with a simulation case study, the safety index in (E3) does not allow the trajectory scaling to be successfully applied in the case of a multi-robot collaborative system as it could lead to conflicting and oscillating situations.

To demonstrate the above, let us consider the same simulation setup of the closest robot approach, shown in Figure 1, composed of two robots ($N = 2$) and a human operator sharing the same workspace. The nominal trajectory, reported in Figure 9, requires both robots moving, in the same direction, along axis x with velocity of robot 2 greater than velocity of robot 1. The nominal individual velocities are also reported in Figure 10 for the sake of clarity. Finally, the human operator moves along the same axis and in the same direction with a velocity greater than robot 1. The human trajectory is also reported in Figure 9 (bottom) and his/her velocity in Figure 10. Minimum safety field $\bar{F}_{min} = 13.5$ is assumed in the case study.

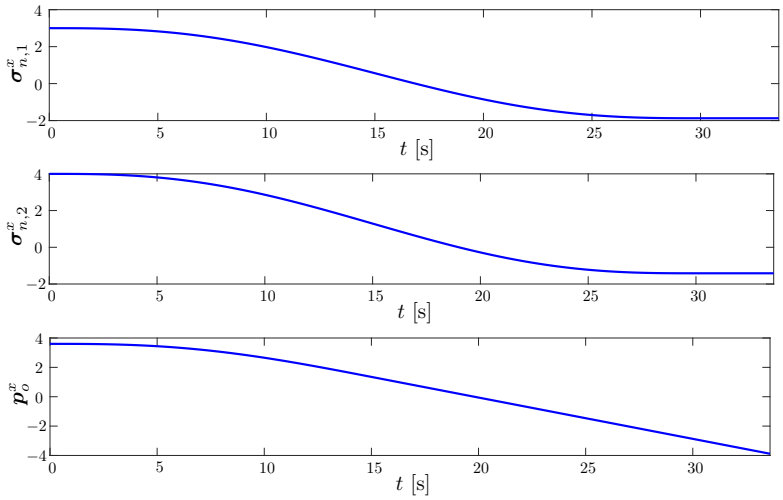

Figure 9: Minimum safety robot approach. Evolution of the nominal positional components along x of the team centroid $\boldsymbol{\sigma}_1$ and formation $\boldsymbol{\sigma}_2$, i.e. $\boldsymbol{\sigma}^x_{n,1}$, $\boldsymbol{\sigma}^x_{n,2}$, and of the human position along x, i.e. $\boldsymbol{p}^x_o$. The components that are not shown are constant.

Simulation snapshots of the nominal behavior and results are shown in Figure 11 and Figures 12-14, respectively. More specifically, the index i_f of the robot with minimum safety index at each time is reported in Figure 12 and the respective overall safety function $\bar{F}$, along with the individual safety

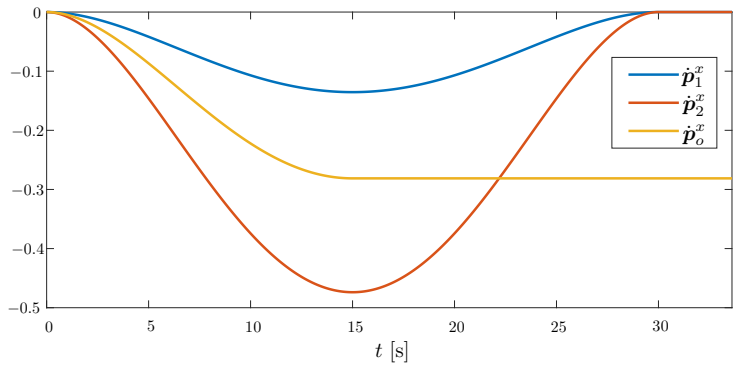

Figure 10: Minimum safety robot approach. Nominal velocities of robot 1 ($\dot{\boldsymbol{p}}_1^x$) and 2 ($\dot{\boldsymbol{p}}_2^x$) and of the human operator ($\dot{\boldsymbol{p}}_o^x$) along x.

functions $\bar{F}_1$ and $\bar{F}_2$, are shown in Figure 13. In addition, the scaling parameters c and derivatives are reported in Figure 14. In particular, until $t = 13.9$ s, robot 2 has minimum safety field, i.e. $i_f = 2$, and, at time $t = 13.1$ s, the trajectory starts to be slowed down accordingly to guarantee the safety condition. However, from time $t = 13.9$ s on, a conflicting scenario arises: both robots are at the minimum value and robot 2 requires to slow down the trajectory, while robot 1 requires to speed it up so as to increase its distance from the human. More specifically, if the trajectory is slowed down, robot 2 becomes the minimum safety one and requires to speed up the trajectory, but at the same time, if trajectory is speeded up, robot 1 becomes the minimum safety one and requires to slow down the trajectory. Oscillations in i_f as well as on the acceleration $\ddot{c}$, which jumps from positive to negative values and viceversa, emerge because of this conflicting behaviors. As a result, the minimum safety $\bar{F}_{min}$ is also not ensured and the task cannot be completed.

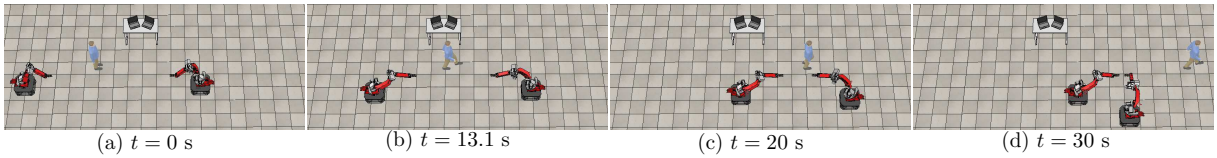

(a) $t = 0$ s (b) $t = 13.1$ s (c) $t = 20$ s (d) $t = 30$ s

Figure 11: Minimum safety robot approach. Snapshots of the key phases of the simulation: the initial configuration of the work-cell is in Figure (a); motion along x of the robots and of the human operator in Figures (b) and (c); final configuration in Figure (d).

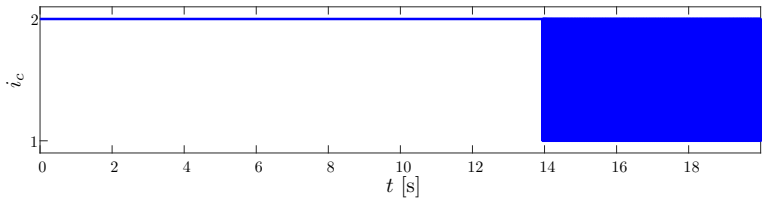

Figure 12: Minimum safety robot approach. Index of the closest robot i_c.

On the contrary, when considering the cumulative safety index presented in the paper the aforementioned problem does not arise by construction.
The approach in Section IV-B with $\bar{F}_{min} = 27.9$, corresponding to $\bar{F} = \bar{F}_1 + \bar{F}_2$ at time $t = 13.1$ s, has been considered. The resulting safety index and the scaling parameters (in blue) compared to their nominal values (in green) are shown in Figures 15 and 16, respectively. In particular, in the time interval [13.1, 20.8] s, the safety index reaches the minimum value $\bar{F}_{min}$ and the trajectory is slowed down; afterwards, the nominal trajectory is restored. The modulated trajectory (in blue) and the respective nominal one (in green) are reported in Figure 17. The proposed method is thus shown to allow the accomplishment of the task.

Finally, it is worth remarking that, for the same reason mentioned in the case of the closest robot approach, this method would also not be suitable for a distributed framework.

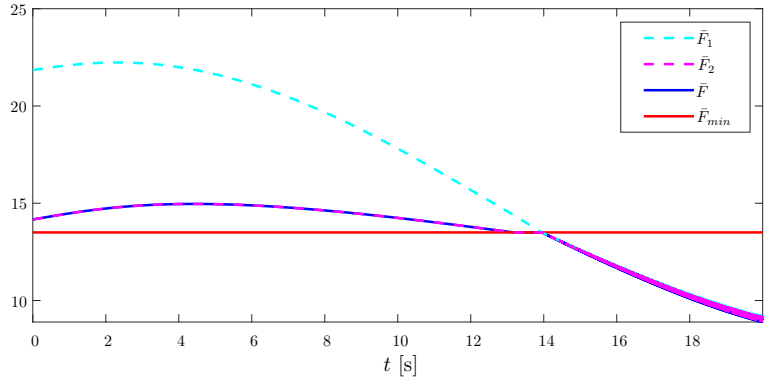

Figure 13: Minimum safety robot approach. Evolution of the overall safety function $\bar{F}$ (solid line in blue) with respect to the minimum allowed value $\bar{F}_{min}$ (in red) and of the local safety functions $\bar{F}_1$ and $\bar{F}_2$ (dotted cyan and magenta lines respectively).

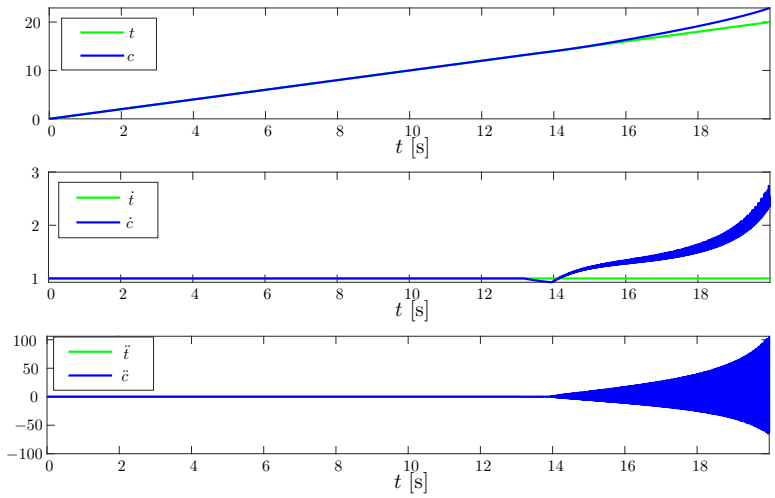

Figure 14: Minimum safety robot approach. Evolution of the scaling parameters $c(t)$, $\dot{c}(t)$, $\ddot{c}(t)$ (in blue) compared with their nominal values (in green).

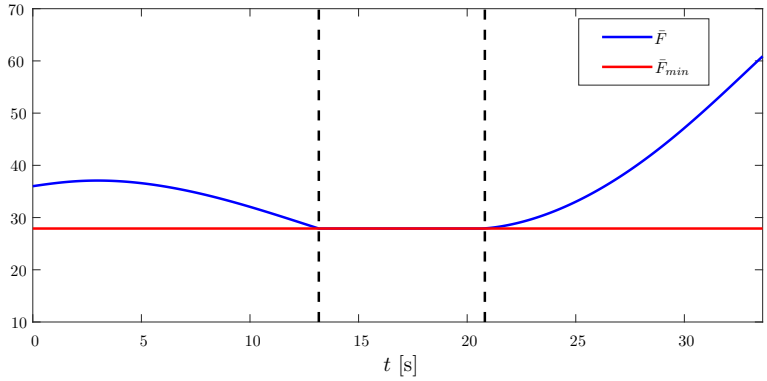

Figure 15: Our method in the setting of the minimum safety robot approach. Evolution of the overall safety function $\bar{F}$ (in blue) with respect to the minimum value $\bar{F}_{min}$ (in red). The scaling phase is highlighted with notation S_c.

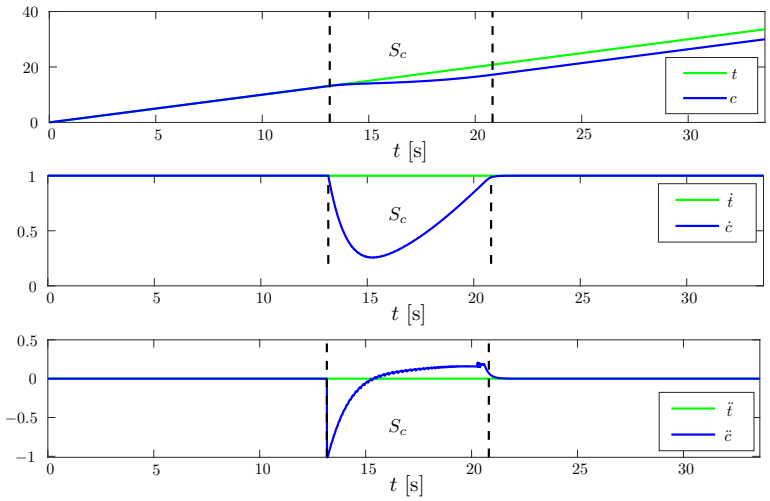

Figure 16: Our method in the setting of the minimum safety robot approach. Evolution of the scaling parameters $c(t)$, $\dot{c}(t)$, $\ddot{c}(t)$ (in blue) compared with their nominal values (in green); scaling phase is highlighted with S_c.

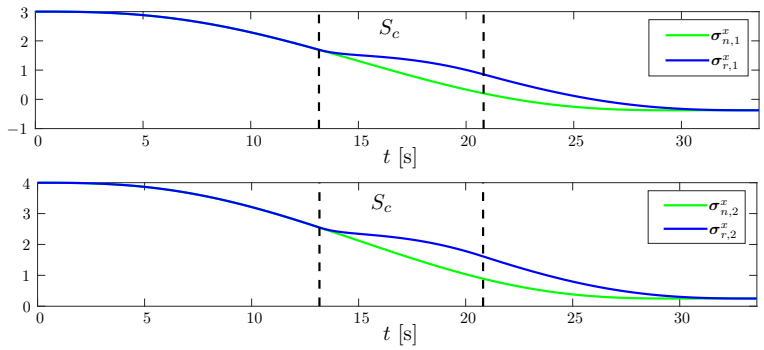

Figure 17: Our method in the setting of the minimum safety robot approach. Evolution of the nominal (n, in green) and reference (r, in blue) trajectories; in detail, the positional components along x of the team centroid $\boldsymbol{\sigma}_1$ and formation $\boldsymbol{\sigma}_2$ are shown (namely, $\boldsymbol{\sigma}^x_{k,1}$, $\boldsymbol{\sigma}^x_{k,2}$ with $k = n, r$). The remaining components are kept constant. Scaling phase is marked with S_c.